Journal of Environmental Chemical Engineering 8 (2020) 103769

Contents lists available at ScienceDirect

Journal of Environmental Chemical Engineering

journal homepage: www.elsevier.com/locate/jece

Ni, C, N, S multi-doped ZrO_2 decorated on multi-walled carbon nanotubes for effective solar induced degradation of anionic dye

Sachin Girdhar Shinde[a], Maheshkumar Prakash Patil[b,c], Gun-Do Kim[b], Vinod Shankar Shrivastava[a,*]

[a] Nanochemistry Research Laboratory, G.T.P. Arts, Commerce, and Science College, Nandurbar 425412, India, Affiliated to Kavayitri Bahinabai Chaudhari North Maharashtra University, Jalgon MH, India
[b] Research Institute for Basic Sciences, Pukyong National University, 45 Yongso-ro, Nam-gu, Busan 48513, Republic of Korea
[c] Department of Microbiology, College of Natural Sciences, Pukyong National University, 45 Yongso-ro, Nam-gu, Busan 48513, Republic of Korea

ARTICLE INFO

Keywords:
Photocatalysis
Multi-doped ZrO_2
Multi-walled carbon nanotubes
Indigo carmine degradation
Scavenger

ABSTRACT

The present work deals with the synthesisis of Ni, C, N, S multi-doped ZrO_2 / MWCNT's nanocomposites varying nickel percentage in ZrO_2 by homogeneous co-precipitation and fabricated on MWCNT's by ultrasound-assisted hydrothermal method. The nanocomposites were characterized by TEM-SAED, SEM-EDAX, XRD, FT-IR and UV–vis techniques. SEM-EDAX, XRD, FT-IR techniques confirmed Ni, C, N and S doping in ZrO_2. The TEM image revealed fabrication of multi-doped ZrO_2 nanoparticles on nanotube surface. The nanocomposites employed for photocatalytic degradation of Indigo Carmine anionic dye in eco-friendly solar radiation. Amongst all nanocomposite 1 % nickel concentarion in ZrO_2 exhibited much higher photocatalytic degradation efficiency (96 %) as compared with bare ZrO_2 (19 %), C,N,S (48 %), 0.3 % (81 %) and 0.6 % (88 %) in 180 min of irradiation at alkaline pH and 3 mgL^{-1} catalyst loading following first order rate kinetics ($K_a = 16.10 \times 10^{-3}$) by virtue of it lower band gap (4.17 eV) confirmed by UV–vis spectrum. The degradation was confirmed by GC−MS and TOC analysis. Synergism of MWCNT's by electron trapping to generate $O_2^{\cdot}$- major species confirmed by scavenger addition experiment. The reusability study demonstrated stability and effectiveness of synthesized material for multiple cycles.

1. Introduction

Clean water is one of the most precious commodity for living organisms on earth including humans. Currently, due to the rapid industrialization, the threat on the water reservoirs is evident [1]. Different types of industries are using various organic chemicals for multiple industrial processes and releasing them into the water bodies [2,3]. Dyes among organic chemicals which are more harmful than others [2]. More than 100,000 types of dyes are synthesized at the rate of 10^5 to10^6 tons per year however, 10–15 % of these dye goes as waste in surrounding water reservoirs like rivers, lakes and eventually in to the oceans [4]. Dyes are highly water-soluble, made up of aromatic origin and very small amount of these can cause serious problems such as absorption of essential sunlight in water bodies, forming residues which incorporate into food chain and show carcinogenic effects, kidney dysfunction, reproductive system problem in humans and other organisms moreover it also increase BOD and COD by decreasing DO in water reservoirs, etc. [2,4,5]. Various techniques such as adsorption, reverse osmosis, nano-filtration, ozone treatment and many more are employed but own limitations such as low efficiency, high cost and secondary waste generation [6,7].

Advanced Oxidation Processes (AOP's) are nowadays promising methods for the complete elimination of organic contaminants from water bodies [8]. Photocatalysts are employed to generate strong oxidizing species like $^{\cdot}OH$, $O_2^{\cdot}$- etc. in the presence of light to carry out AOP's [8,9]. However, AOP's also have some drawbacks such as the need of proper light energy source, less utilization of visible radiation which is 93–95 % of total solar radiation, use of high cost and low yield catalysts and inefficiency in working on a pilot-scale [9,10]. To avoid these short comes, the eco-friendly process of AOP's by using solar radiation and visible light harvesting development of photocatalyst is needed [10]. Many workers have developed photocatalyst originated from TiO_2 and ZnO systems however, many others are yet to be investigated [5,6]. ZrO_2 is one of the strongest contender as a

* Corresponding author at: Nanochemistry Research Laboratory, G.T.P. Arts, Commerce, and Science College, Nandurbar 425412, India, Affiliated to Kavayitri Bahinabai Chaudhari North Maharashtra University, Jalgon MH, India
E-mail address: drvinodshrivastava1962@gmail.com (V.S. Shrivastava).

https://doi.org/10.1016/j.jece.2020.103769
Received 22 December 2019; Received in revised form 6 February 2020; Accepted 8 February 2020
Available online 09 February 2020

photocatalyst by virtue of its low cost, nontoxic effects, stability at high temperature, strength and re-usability [11–13]. However, poor sensitivity towards UV–vis light due to large bandgap (5.00–5.18 eV), slow generation and rapid recombination of electron-hole pair (e^-/h^+) are some major drawbacks of ZrO_2 systems [14,15]. One of the most effective method to reduce these flaws is by doping these less efficient metal oxides systems with metal and non-metal dopant's [14,16,17].

Metal dopant's shift the absorption to UV–vis range by decreasing the bandgap energy, improve morphology, surface properties and facilitate generation of e^-/h^+ pair [16,18]. Nickel is an ideal dopantt in transition series by virtue of its wide band gap (3.6 eV–4.0 eV). Moreover, Ni^{2+} has effective ionic radii 72 pm which is less than Zr^{4+} (80 pm) which favor's the incorporation of Ni^{2+} ions in the ZrO_2 system. NiO is also a p-type of dopant helps to form p-n junction with base metal oxide and increase separation of photo induced charge carriers (e-/ h^+ pair). In addition, large accessible surface area and homogenous distribution of dopants in particles are favorable for the enhancement of photocatalytic activity of doped ZrO_2 [19,20]. Non-metal introduced by simple precursors like urea, thiourea, various amino acids, etc. maximize the generation of e^-/h^+ pair due to interaction of 2p levels of non-metals with 2p levels of oxygen in metal oxide [21,22], decrease the recombination of these photoinduced charge carriers and eventually increase the efficiency of photocatalyst [22].

Recently, introduction of carbonaceous materials to form composites have been extensively practiced and has shown exceptional improvement in photocatalytic ability of less effective metal oxide systems [23,24]. Graphene based materials are one of the most important additions to this tally due to their excellent thermal conductivity, high surface area and high thermal and chemical stabilities [25]. GO and rGO are also employed due to their large specific surface area, high charge carrier mobility and photosensitizing capacity [26]. Moreover, presence of oxidizing group on GO surface help it to disperse in aqueous medium to show its activity, [27,28]. Currently, focus is also shifted on introduction of three dimensional CNT in place of these two dimensional graphene based materials [29]. This is due to their similarities with GO such as, photosensitizing capacity, large surface area with high adsorption capacity due to their 3D structure. Besides, they also support nanomaterial to increase its strength and maximize overall surface area for nanomaterial and subsequently enhance photodegradation capacity [4,30,31]. This synergism of increasing active sites by increasing surface area, trapping of an excited electrons to avoid recombination makes carbon nanotube a significant factor in increasing the photocatalytic activity of an ineffective metal oxide systems [31,32].

In the current study, metal and non-metal doped ZrO_2 nanoparticles were synthesized by varying nickel concentration from 0.3 to 1.0 (%w) by hydrothermal co-precipitation method. The synthesized C,*N*,S and Ni,C,*N*,S ZrO_2 were fabricated on the MWCNT's to form C, N, S and Ni, C, N, S multi-doped ZrO_2 / MWCNT's nanocomposites by ultrasound-assisted hydrothermal method and characterized by SEM, TEM-SAED, XRD, FT-IR and UV–vis techniques. Then, the synthesized nocomposites were employed for the degradation of Indigo Carmine anionic dye under eco-friendly solar radiation. In addition, the operational parameters such as effect of pH, catalyst dose, effect of dopant concentration and reaction kinetics were also investigated. The degradation efficiency was also studied by GC–MS and TOC techniques. Moreover, the reaction mechanism and detection of active oxidizing species by scavenger addition and reusability of the most effective nanocomposite was also investigated.

2. Material and methods

2.1. Materials

All chemicals used without further purification. Zirconyl oxy nitrate ($ZrO(NO_3)_2$) (97 %) (Sigma Aldrich, Mumbai, India), Nickel (II) nitrate hexahydrate ($Ni(NO_3)_3{\cdot}6H_2O$), Nitric acid (HNO_3), Indigo Carmine (IC), Sodium Hydroxide (NaOH), Hydrochloric acid (HCL), Sodium Chloride (NaCl) purchased from Fisher Scientific, Mumbai, India. Carbon Nanotubes Multi-walled (OD: 10–20 nm, Length 30–90 nm) made available by Sisco Research Laboratories Pvt. Ltd. Mumbai, India. Thiourea, $CS(NH_3)_2$ (99 %) and Polyethyleneglycol - 200 (99.9 %), Isopropyl alcohol, EDTA, Benzoquinone were purchased from Merk, Nashik, India.

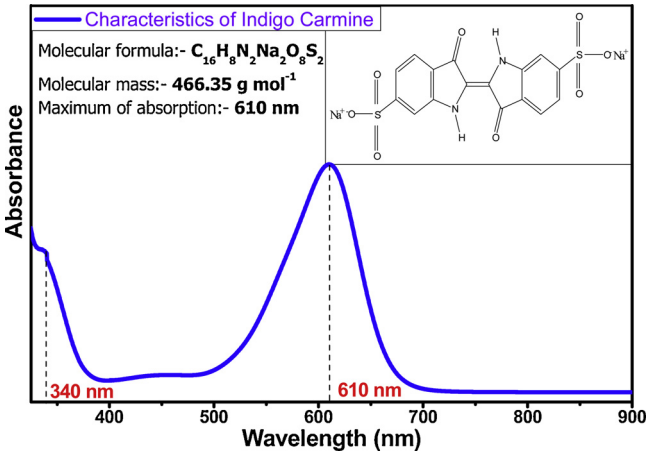

Fig. 1. Characteristics of Indigo Carmine dye.

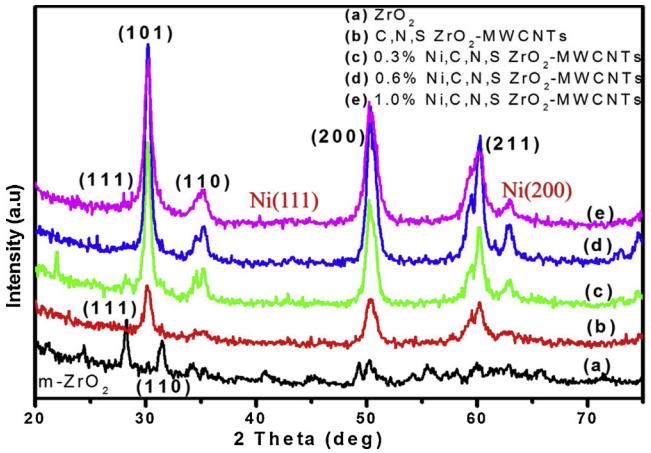

Fig. 2. XRD pattern of bare ZrO_2, C,N,S ZrO_2CNT and Ni,C,N,S ZrO_2CNT (0.3, 0.6,1.0 % Ni).

2.2. Preparation of dye solution

Indigo Carmine dye (IC) Fig. 1 was used as an organic contaminant. The stock solution (100 mg L^{-1}) of IC was prepared using double distilled water. The desired concentration of dye solutions was prepared by serial dilution of prepared stock solution with double distilled water.

2.3. Catalyst preparation

2.3.1. Synthesis of the C,N,S and Ni,C,N,S multi-doped ZrO_2 (CNSZr) and (NiZr)

Ni, C, N, S multi-doped ZrO_2 (NiZr) was prepared by adding ($ZrO(NO_3)_2$) (1.0 mM) to 0.1 mol L^{-1} 100 mL HNO_3 solution. Then, dropwise polyethylene glycol-200 (1.0 mL) was added and the mixture was stirred for 1 h. Thereafter, a calculated amount of $Ni(NO_3)_2{\cdot}6H_2O$ by considering Ni:Zr ratio as 0.3 %, 0.6 %, and 1.0 % was added and stirred for 1 h. Then, thiourea (3 g) was added and the mixture was stirred for 2 h. The homogeneous solution was dried in an open-air oven

Table 1
Crystallite size for commercial ZrO_2 and synthesized nanocomposites from (111) and (101) peak with average crystallite size of 1.0 % Ni,C,N,S ZrO_2/ MWCNT's.

Photocatalyst	Peak type	FWHM (β)	Crystalline Size (D)(nm)
ZrO_2	(111) m-ZrO_2	1.0150	8.51
C,N,S ZrO_2/MWCNT's	(101)	0.8900	9.72
0.3 %Ni,C,N,S ZrO_2/MWCNT's	(101)	0.8202	10.53
0.6 %Ni,C,N,S ZrO_2/MWCNT's	(101)	0.8411	10.26
1.0 %Ni,C,N,S ZrO_2/MWCNT's	(101)	0.9819	8.84
1.0 %Ni,C,N,S ZrO_2/MWCNT's	(101)	0.9819	8.84
1.0 %Ni,C,N,S ZrO_2/MWCNT's	(200)	0.2698	32.28
1.0 %Ni,C,N,S ZrO_2/MWCNT's	(211)	3.7076	2.55
	Average Crystallite Size		**14.55 nm**

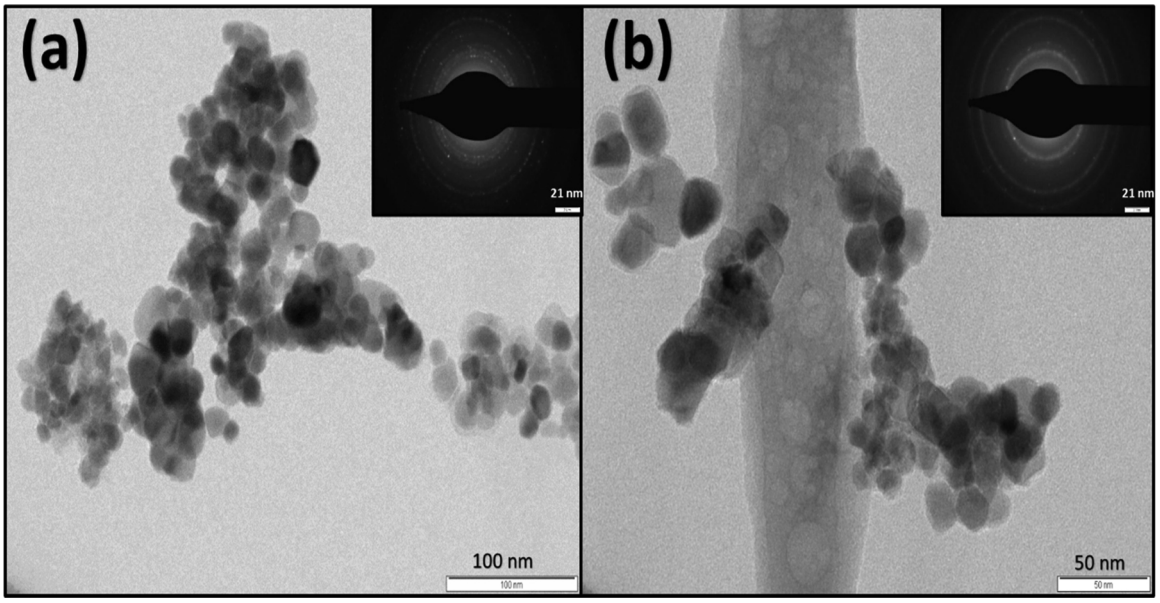

Fig. 3. (a) TEM image of 1 % Ni,C,N,S ZrO_2 and **(b)** TEM image of 1.0 % Ni CNSZrCNT, Inset SAED pattern of prepared materials.

at 100 °C for 12 h. The black residue obtain was calcined at 500 °C for 3 h to obtain a white powder of Ni, C, N, S doped ZrO_2. The metal-free C,*N*,S multi-doped ZrO_2 was synthesized by following the same procedure by eliminating addition of the nickel precursor denoted as CNSZr [11,33].

2.3.2. Synthesis of the C,N,S and Ni,C,N,S multi-doped ZrO_2 / MWCNTs nanocomposite (CNSZrCNT) and (NiZrCNT)

The C,N,S (CNSZrCNT) and Ni,C,N,S multi-doped ZrO_2/MWCNTs (NiZrCNT) nanocomposites were synthesized by ultrasound-assisted hydrothermal method by dispersing 0.05 g of MWCNTs and 0.50 g of previously synthesized CNSZr and NiZr in 80 ml 20 % ethanol under ultrasonic treatment for 3 h with vigorous stirring. Then the suspension was placed in 100 mL teflon-lined stainless steel autoclave and the pH value was adjusted to 2–3 with concentrated nitric acid and kept for 12 h at 140 °C. The suspension then allowed to cool at room temperature and the product was isolated by centrifugation and washed several time with ethanol and double distilled water, then dried at 100 °C for 10 h [34]. The nanocomposites obtained denoted as C,N,S (CNSZrCNT) and Ni,C,N,S multi-doped ZrO_2/ MWCNTs (NiZrCNT).

2.4. Characterization

The morphology, grain size, crystallinity and phase composition of the nanocomposites were characterized by transmission electron microscopy (TEM) with selected area electron diffraction (SAED) and X-ray diffraction (XRD) techniques. The XRD study was carried out with a monochromatic high-intensity Cu Kα radiation (1.54060 Å) and X-ray diffractometer 45 kV & 40 mA with a goniometer radius 240 mm. The intensity data were collected at 25 °C in a 2θ range from 20° to 90° having slit size 0.8710° with the angular type of slit opening with step size of 0.017° 2θ and continuous scanning rate of 0.1° s^{-1}. The TEM analysis was carried out by Philips model CM 200. The morphology, crystallite size, porosity and composition of synthesized materials was detected by the field–emission scanning electron microscopy (FESEM) and energy dispersive X-ray (EDAX) by model JSM 7600 F. Various functionalities were identified by Fourier transform infra-red spectroscopy (FT-IR) by 3000 Hyperion Microscope with Vertex 800 FT-IR System, Bruker, Germany. The UV–vis absorbance and dye absorbance was recorded by Jasco V-730 double beam spectrophotometer.

3. Results and discussions

3.1. XRD analysis

The crystallinity and phase composition of the nanocomposites was studied by XRD analysis. Fig. 2 shows the XRD pattern of bare ZrO_2, CNSZrCNT and 0.3, 0.6, 1.0 % nickel doped NiZrCNT. The sharpness of the peaks in Fig. 2 shows highly crystalline in synthesized nanocomposites and the pattern indicates the presence of multiple monoclinic and tetragonal crystalline phases of ZrO_2 system. Commercial ZrO_2 in Fig. 2 a. shows peaks at 27.34° and 30.58° indexed to (111) and (110) planes are the characteristic peaks of typical monoclinic ZrO_2 (m-ZrO_2) [35,36], on the other hand in synthesized composites the peaks at

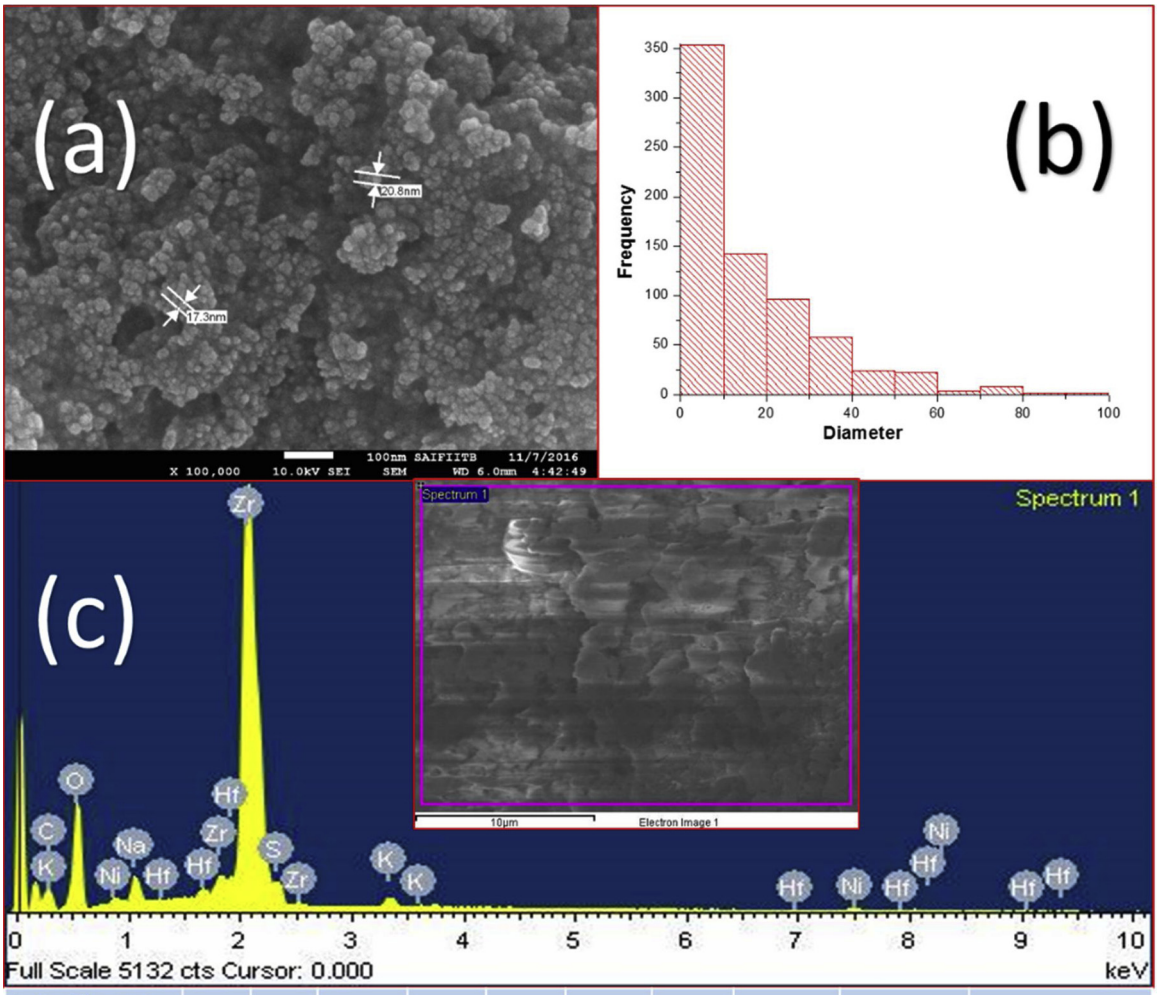

(d)

Element	C K	N K	O K	S K	Ni K	Zr L	Hf M	Na K	K K	Total
Weight%	9.31	1.03	25.52	1.95	1.26	57.18	1.31	1.50	0.94	100

Fig. 4. (a) SEM image, **(b)** Particle size distribution histogram, **(c)** EDAX analysis and **(d)** Elemental composition (w%) of 1.0 % Ni,C,N,S ZrO_2CNT.

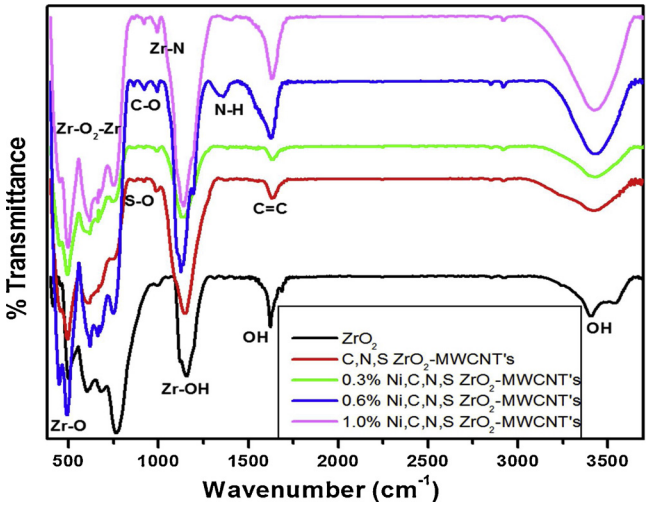

Fig. 5. FT-IR transmittance spectrum of ZrO_2, C,N,S ZrO_2CNT and Ni,C,N,S ZrO_2CNT(0.3,0.6,1.0 %Ni).

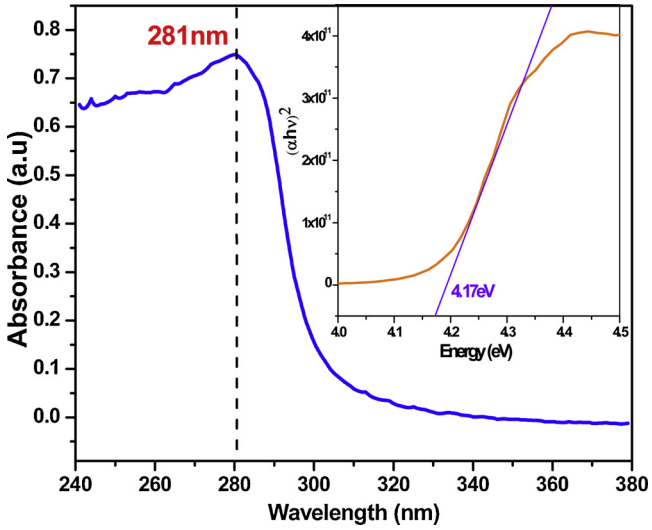

Fig. 6. Uv–vis absorbance and Tauc plot of 1.0 % Ni,C,N,S ZrO_2CNT.

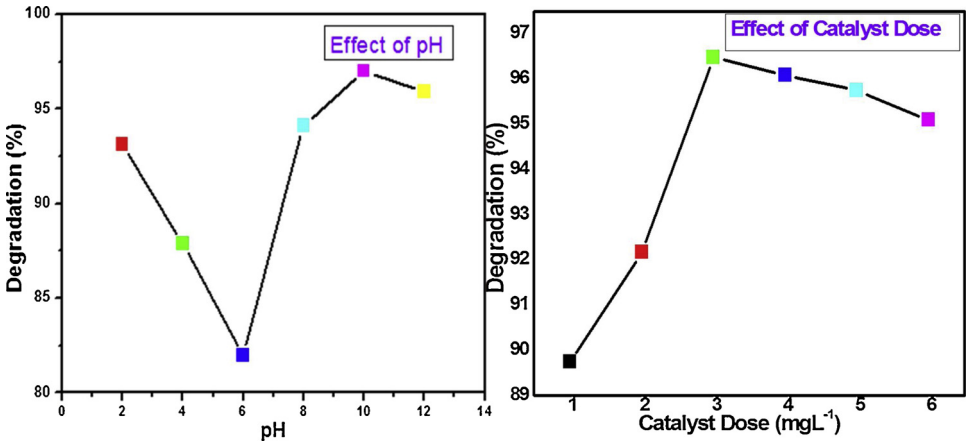

Fig. 7 and Fig. 8. Effect of pH and Effect of Catalyst Dose on photocatalytic degradation of IC by 1.0 % Ni,C,N,S ZrO_2CNT.

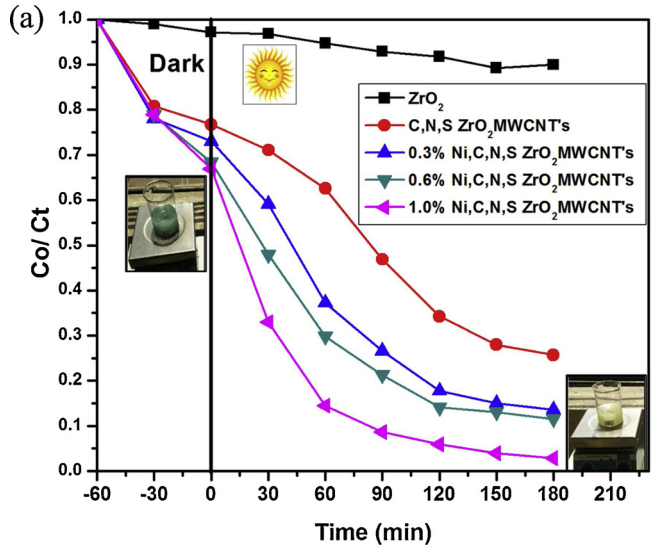

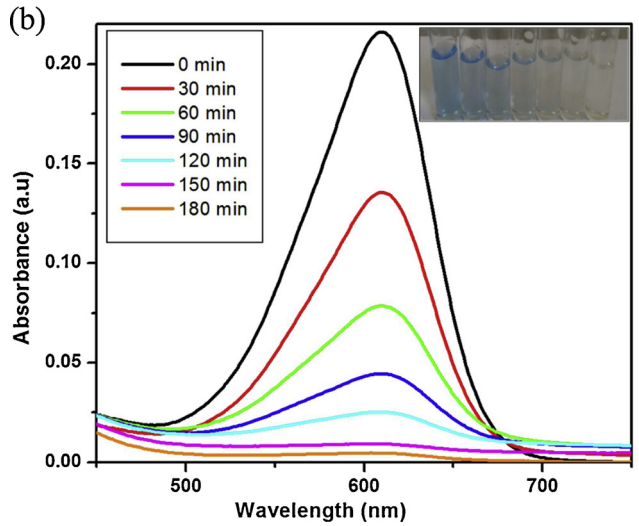

Fig. 9. (a) Indigo carmine photodegradation profile of ZrO_2, C,N,S ZrO_2CNT and Ni,C,N,S ZrO_2CNT (0.3, 0.6, 1.0 % Ni) under solar irradiation. **(b)** Indigo carmine decolorization profile using 1 %Ni,C,N,S ZrO_2CNT.

29.34°, 49.50° and 59.33° indexed to (101), (200) and (211) respectively attributed to tetragonal ZrO_2 (t- ZrO_2) phases and the increase in peak sharpness attributed the shift towards high crystallinity of nanocomposites [36,33].

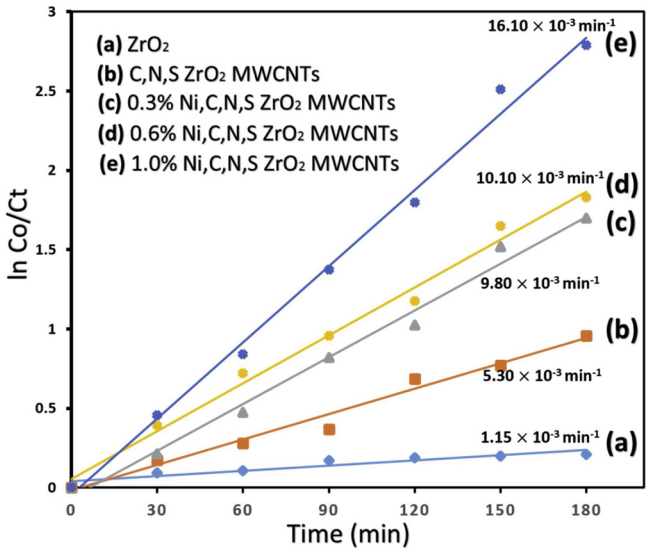

Fig. 10. Kinetics of Indigo carmine photodegradation by ZrO_2 C,N,S ZrO_2CNT and Ni,C,N,SZrO_2CNT (0.3, 0.6, 1.0 % Ni).

Table 2
First order decolorization rate constant of IC dye by 1.0 %Ni, C, N, S ZrO_2CNT.

Photocatalyst ($3\ mg\ L^{-1}$, IC- $10\ mg\ L^{-1}$)	Rate Const.(K_a) min^{-1}	Linear regression coefficient (R^2)
ZrO_2	1.15×10^{-3}	0.9513
C,N,S ZrO_2 / MWCNT's	5.30×10^{-3}	0.9778
0.3 %Ni,C,N,S ZrO_2 / MWCNT's	9.80×10^{-3}	0.9889
0.6 %Ni,C,N,S ZrO_2 / MWCNT's	10.10×10^{-3}	0.9906
1.0 %Ni,C,N,S ZrO_2 / MWCNT's	16.10×10^{-3}	0.9917

Nanocomposites patterns indicate the tetragonal phase is more dominant in the nanocomposites than a monoclinic phase. However, a small amount of m-ZrO_2 phase is evident from the peak 39.65° indexed to (110) (37). The characteristic Ni-base phase that is 37.2° and 43.2° corresponding to (111) and (200) [38,39] merged into ZrO_2 diffraction planes except in Fig. 2 e. for 1.0 % nickel concentration, however, as the Ni percentage increased the peak at 49.50° indexed to (200) has slightly shifted toward right confirming the incorporation of nickel in ZrO_2 lattice [38]. The peak at 62.08° for NiO corresponding to (220) is evident in all XRD peaks of nickel doped ZrO_2. The dominancy of NiO phase in synthesized material as compared to the metalic Ni is due to

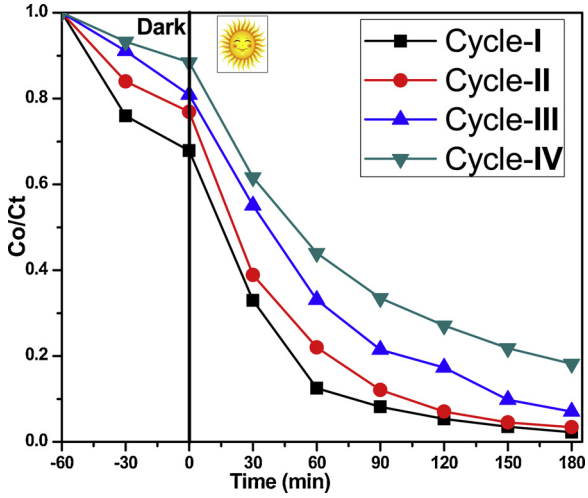

Fig. 11. Reusability of 1 % Ni,C,N,S ZrO_2CNT for four cycles.

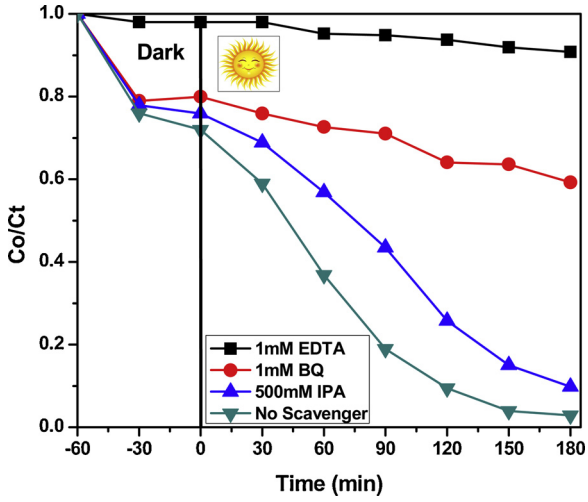

Fig. 12. Effects of different scavengers on the degradation of Indigo Carmine in the presence of 1 %Ni,C,N,S ZrO_2CNT under solar irradiation.

the low calcination temperature employed for the synthesis of multi-doped ZrO_2 (500 °C), higher calcination temperature greater than 700 °C converts NiO in to metallic Ni [40]. The typical (002) plane at about 25° of hexagonal graphite from MWCNT is not visible in the pattern may be due to the strong shielding of m- ZrO_2 [16,41].

The average crystallite size of nanocomposites was calculated by Debye–Scherrer's formula Eq. [1]. by considering high intense peaks.

$$D = \frac{0.94\,\lambda}{\beta\,\mathrm{Cos}\,\theta} \quad (1)$$

Where, λ is 1.54060 Å, K is constant = 0.94, B is FWHM (Full Width Half Maxima) and θ is diffraction angle (Cu-Kα) [32].

The varities of crystallite size value of the nanocomposites were found from XRD high intense peaks. Table 1.summarizes the crystallite sizes of all synthesized CNSZr and NiZrCNT nanocomposites calculated from (101) and for m-ZrO_2 (111) line broadening and average cryastallite size of 1.0 % NiZrCNT's from (101), (200), (211) peaks [42,43]. Size variation in the synthesized materials with doping is distinct and proved the doping affected the crystallite size of all the synthesized materials [44].

3.2. TEM and SAED pattern analysis

TEM analysis carried out to analyze the microstructure and morphology of prepared nanocomposites. The TEM image of the prepared nanomaterial and nanocomposite revealed essential information about the functionalization of MWCNTs. Fig. 3 a is the TEM image of 1 % Ni, C,*N*,S doped ZrO_2 (NiZr) which are spherical in nature and show heterogeneous nanosphere morphology. Fig. 3 b shows the coating of prepared NiZr on the surface of MWCNT in clusters and in the form of single crystals can be seen as white spots on the wall of a nanotube [30]. The coating will certainly help to increase the surface area of as prepared NiZr and CNSZr [16,30]. The MWCNT functionalization will synergize with the nanospheres to enhance the photocatalytic efficiency by sensitization and trapping the excited electrons to avoid recombination [45]. The SEAD pattern of both the materials is given in the inset of Fig. 3 a, b revels high crystallinity and well-defined pattern of ring structure in Fig. 3 a (inset) [42] The pattern in Fig. 3 b (inset) shows typical graphene type blurring of the ring confirming the presence of nanotubes to form nanocomposite [44].

3.3. SEM and EDAX analysis

SEM-EDAX was performed to understand the morphology, particle size and elemental composition in the synthesized 1.0 % NiZrCNT nanocomposite. The surface morphology was found in high-resolution SEM images related to agglomerated nanospheres. It is evident from SEM image Fig. 4 a that the particle size is heterogeneous and a large number of cavities are observed which indicate high porosity in the 1.0 % NiZrCNT [46]. The highly interconnected porous material with consistent crystallite size shows high adsorption capacity and surface area which eventually increase the photocatalysis process [32,47]. The SEM image and particle size distribution studies reveled the average crystallite size is within 6–20 nm (Fig. 4 b) is in close agreement with the crystallite size calculated from XRD (14.55 nm) for 1.0 % NiZrCNT.

The EDAX analysis revealed the elemental composition of 1.0 % NiZrCNT. The spectra in Fig. 4 c shows the successful incorporation of various non-metals and metals into the ZrO_2 system. The weight percentage of carbon due to the MWCNT's is 9.31(w%) and for sulphur and nitrogen 1.95 and 1.03 respectively. Nickel percentage 1.26 showing successful doping of 1.0 % nickel ions in ZrO_2 major oxide which is 57.18 (w%) Fig. 4 d.

3.4. FT-IR analysis

FT-IR spectroscopy gives information about the chemical bonding in a material. The FT-IR spectrum Fig. 5 of materials were recorded in the range 4000–400 cm^{-1} and reveled essential information related to metal, non-metal and CNT functionalities. The characteristic broad peak observes between 3435 to 3400 cm^{-1} due to the presence of physically and 1630 to 1625 cm^{-1} for bending vibrations of chemically adsorbed water molecules [48]. The broadening of peak compare to m-ZrO_2 around 1630 cm^{-1} due to C═C bonding is evident due to sp^2 carbons in nanotubes as prepared nanocomposite [49,50]. The peak 1150 to 1140 cm^{-1} in all spectra represents the Zr − OH bonding with the peaks within 580 to 450 cm^{-1} indicate the ZrO-Zr and Zr-O bonding in synthesized materials [51]. The characteristic frequencies of Ni-O within 615–605 cm^{-1} are merged into this broadband absorption range of ZrO-Zr and Zr-O bonding [11,52]. The small peaks at 1111 cm^{-1}, 1116 cm^{-1} and 1170 cm^{-1} which are absent in pure ZrO_2 attributed to S—O, C—O and Zr-N stretching frequency respectively confirm the presence of C, N, S [47,48,53,54]. The bending vibration peak of N—H appear at 1455 cm^{-1} again confirms the presence of nitrogen [47]. The FT-IR information is enough to confirm presence of dopant's in all synthesized nanocomposites.

3.5. Optical property

The UV–vis absorption spectrum of 1.0 % NiZrCNT was recorded (Fig. 6). The crystallite size, changes in morphology and structural

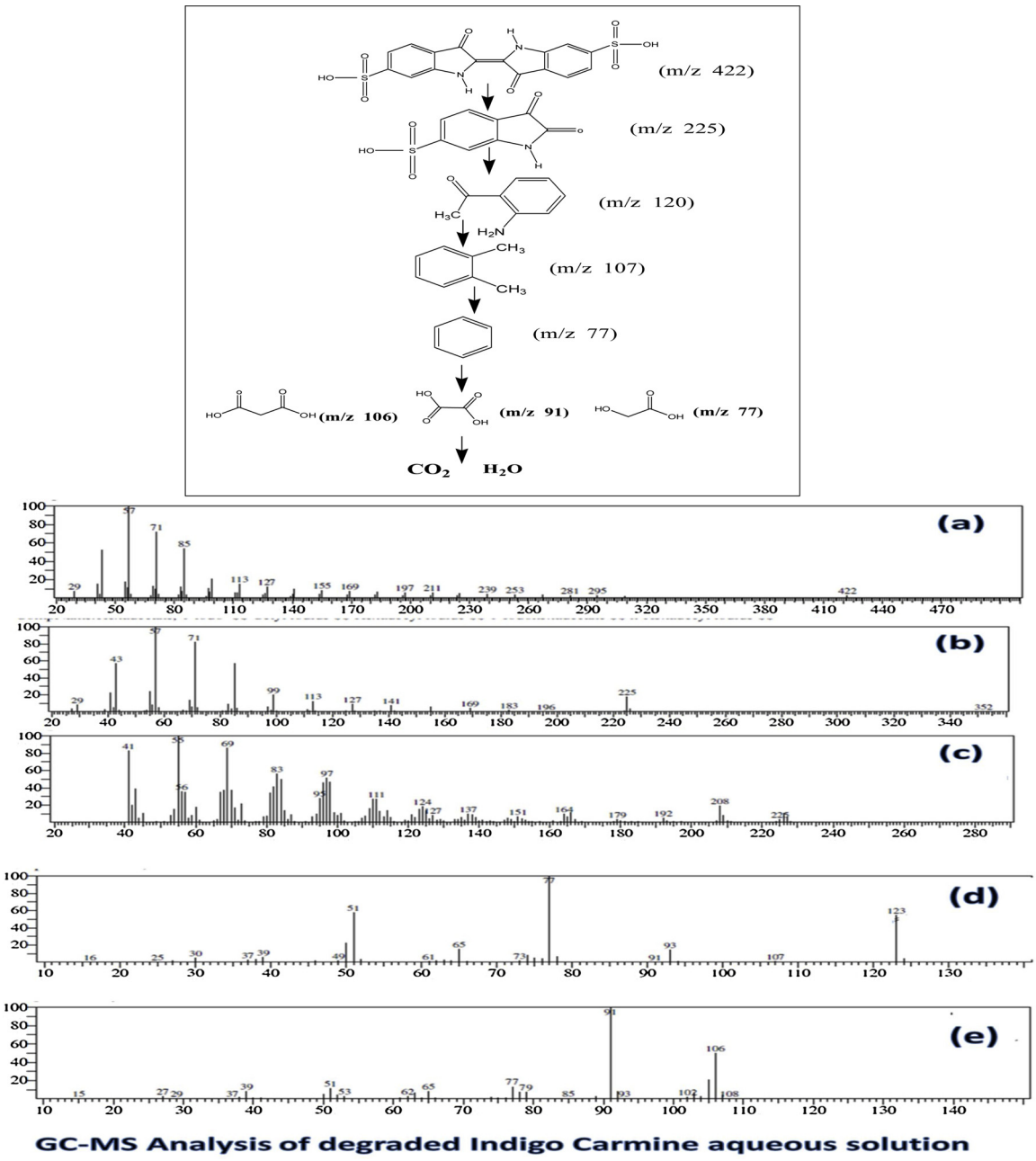

Fig. 13. GC–MS analysis and probable metabolites of IC degraded solution.

defects affect the bandgap [33]. In ZrO_2 system, oxygen electrons to zirconium ion charge transfer are responsible for the absorbance at 200–250 nm [14,30]. The nickel and C,*N*,S doping, in this case, shifts the absorption maxima towards a hypsochromic (blue) shift to 281 nm [48]. Tauc plot (Fig. 6 inset) of 1.0 % NiZrCNT indicates the bandgap of material 4.17 eV is less than the bare ZrO_2 which is in the range of 6.3–6.4 eV [37,48]. Eq. [2]. used to find the bandgap.

$$\alpha(h\nu) = C(\ h\nu - \ Eg)m/2 \tag{2}$$

Where, α is the absorption coefficient, *C* is constant, *hν* photon energy. The energy intercept of a plot of $(\alpha h\nu)^2$ vs. *hν* yields Eg for a direct transition (m = 1) and gives the band gap energy of 1.0 % NiZrCNT nanocomposite.

4. Photocatalytic studies

The eco-friendly solar radiation was utilized as an energy source for photocatalytic study. The time was chosen from 12:00 AM to 15:00 PM when the solar irradiation is consistent and ranged from 1155 to 870 W/ m^2 recorded by digital solar sun meter indicating the major visible part of solar flux. Various parameters were tested by placing the reaction assembly in the solar radiation. The degradation percentages of IC were calculated by the following Eq. [3] [55].

$$\%\ \text{Degradation} = (1 - \frac{Ct}{Co}) \times 100 \tag{3}$$

Where C_o is concentration of IC before irradiation and C_t is the concentration after a certain irradiation time.

4.1. Effect of pH of the solution

pH is an essential factor in the degradation process since, it influences the surface reactions, adsorption and generation of oxidizing species in solution [56]. The point zero charge (pHpzc) of the 1.0 %

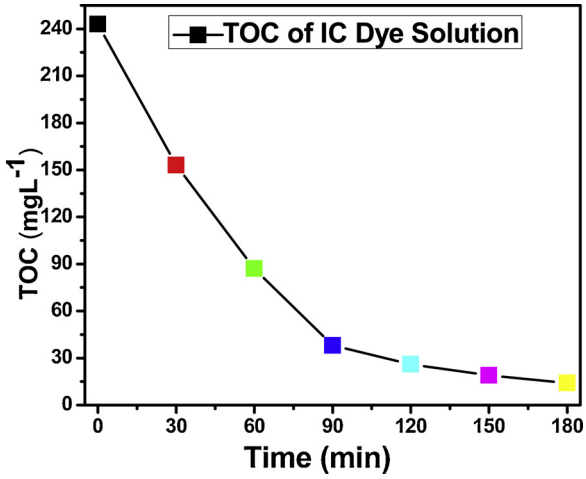

Fig. 14. TOC analysis of degradaed IC dye solution for different intervals of time.

NiZrCNT were determined by using 1 N NaCl solution by monitoring the change in pH for 72 h [57]. The pHpzc value obtained from the experiment was 4.2. At this pH, the photocatalyst surface acquires net-zero charges. When the pH of a solution is below 4.2 the surface of the photocatalyst is positively charged and when it is greater than 4.2 the surface is negatively charged Eq. (4). [33,57].

$$M-OH2 + \longleftarrow (< pH4.2)M\text{–}OH\ (>pH4.2) \rightarrow M-O- \quad (4)$$

The effect of pH on degradation efficiency was studied by loading 1.0 % NiZrCNT by varying the pH from 2 to 12 of IC dye aqua solution with the help of 0.1 N HCl and 0.1 N NaOH before introducing photocatalyst. The highest degradation was observed at pH 4 and pH 10. The lower pH favors adsorption followed by degradation and degraded dye almost 90 % is evident because of the surface phenomenon which is discussed previously [57]. The basic pH 10 shows 96 % of degradation probably due to the increase in the generation of $^{\cdot}OH$, $O_2^{\cdot}$- radicals which are major oxidizing species for degradation [58]. Above pH 10 slight decrease in the efficiency probably due to the formation of carbonates and bicarbonates anions from photo-generated CO_2 which are known scavengers of reactive species (Fig. 7) [59].

4.2. Effect of catalyst dose

The appropriate catalyst concentration was optimized before the comparison of all the synthesized nanocomposites by using 1.0 % NiZrCNT, pH of 10 mg L^{-1} IC dye solution was adjusted to 10 and 1–6 mg L^{-1} catalyst was loaded. It is obvious that the dye degradation percentage increases with an increase of the amount of 1.0 % NiZrCNT up to a limit above which no improvement is obtained. The minimum catalyst dose for complete degradation was found 3 mgL^{-1} thereafter, no appreciable increase was observed. At 1 mg L^{-1} 87 % degradation was obsrved, at 3 mgL^{-1} 96 % degradation is achived, on the other hand at 6 mg L^{-1} the degradation efficicency was decresed by almost 4 %. This was probably due to an increasing opacity of the suspension, unavailability of dye molecules, increase in light reflectance and less penetration of light into the dye solution due to the saturation of catalyst particles (Fig. 8) [60].

4.3. Comparison of prepared photocatalysts

The efficiency of the prepared nanocomposites was tested by photocatalytic degradation of 100 mL solution of 10 mg L^{-1} of IC. The pH was adjusted to 10 and 3 mgL^{-1} of the catalyst was introduced into the solution. The resulting solution was kept in dark for 60 min at continuous stirring to attain adsorption-desorption equilibrium and the suspension immediately placed in solar light. The aliquot from the reaction mixture were taken after intervals of 30 min and subjected to centrifugation for 5 min to eliminate the interference of catalyst. The supernatant solution was removed by a clean syringe and placed into quartz covet and absorbance recorded at λ_{max} = 610 nm by double beam spectrophotometer.

It was observed amongst the nanocomposite 1 % nickel concentarion exhibited much higher photocatalytic degradation efficiency (96 %) as compared with 0.3 %(81 %), 0.6 % (88 %), C,*N*,S (48 %) and bare ZrO_2 (19 %) in 180 min of solar irradiation. (Fig. 9 a and b). The nickel percentage was proved essential for the efficiency of catalyst for 96 % degradation of IC dye. The first-order relationship of IC degradation is observed by plotting the graph ln C_o /C_t versus time t (Fig. 10). The introduction of C,*N*,S in ZrO_2 increase the degradation much more than bare ZrO_2 and by introducing nickel ions the degradation efficiency shooted up with rate constant $K_a = 16.10 \times 10^{-3}$ min^{-1} for 1.0 % NiZrCNT where, bare ZrO_2 showed K_a value 1.15×10^{-3} min^{-1} (Table 2). The efficiency of the catalyst was directly proportional to the percentage of nickel in the prepared photocatalyst.

This remarkable change in rate of degradation is probably attributed to introduction of non-metals like C,*N*,S which increase excitation of electrons due to the overlap of O2p levels of ZrO_2 with 2p levels of non-metals and by decreasing electron-hole recombination. Moreover, they shift the absorption towards UV–vis range [25]. NiO which is predominant the metallic Ni in to the ZrO_2 system due to low calcination temperature (500 °C) decrease the bandgap energy due to ZrO_2 n-type and NiO p-type p-n junction which restricts the recombination of electron-hole pair, change the optical shift due to this electric junction field. Besides, it also improve the crystallite size and increase overall surfece area [33,61]. MWCNT's increase adsorption of dye molecule on surface of CNT and make it available for degradation by synergic effect [4,44].

4.4. Reusability of photocatalyst

The efficiency and stability of synthesized nanocomposites were tested by the reusability experiment. After each photocatalytic

Table 3
Comparison of catalytic ability of ZrO_2 photocatalysts.

Dopant	Fabrication method	Pollutant	Radiation source	Degradation efficiency (%)	Ref.
NiO-ZnO	Sol-gel	Reactive blue 81	15W (UV-C) Hg lamp 254nm	97.6 % in 180 min	[76]
Nd and Graphene oxide	Homogeneous co-precipitation	Eosin Y	Sunlight	~95 % in 180 min	[77]
Sm_2O_3 and Eu_2O_3	Hydrothermal method	*p*-nitrophenol	UV light	90.4 % in 100 min	[78]
Pt and Pd	Impregnation technique	Indigo disulfonate	UV light	97 % in 14h	[79]
Bi and La	Sol-gel	Methylene Blue	Sunlight	~70 % in 240 min	[80]
SiO_2	Sol-gel	Methylene Blue	UV light + O_3	~96 % in 100 min	[81]
Ni,C,N,S and MWCNT	Homogeneous co-precipitation	Indigo Carmine	Sunlight	96 % in 180 min	[This work]

experiment that is the first cycle, the 1.0 % NiZrCNT catalyst was filtered, washed several times with water and ethanol separately and kept for drying at 80 °C for 3 h in an open-air oven thereafter, the catalyst was recovered and collected in silicon crucible and dried in muffle furnace at 150 °C for 2 h [62]. The recovered catalyst was subjected to the degradation by keeping pH 10 of 10 mg L^{-1} IC solution under solar radiation (Fig. 11). The adsorption and catalytic efficiency of the catalyst were substantial up to three cycles eventually decreased up to 9 % which is probably due to minimization of active catalytic surface and loss of catalyst during the recovery process [63]. Furthermore, the degraded dye solutions of first and fourth cycle were tested to check wether the leaching of nickel ions is taken place during degradation process by a spectrophotometric method modified by the inclusion of the ethylenediaminetetraacetate (EDTA) solution as a chromogenic reagent reported by Yongnian Ni et al. It was observed that no change in absorption spectra in both the solution was found as compared to blank EDTA buffer solution. If solutions had nickel ions in it, the spectra would have been shifted to 380 and 590 nm due to the complex formation with EDTA [64].

4.5. Photocatalytic mechanism

It is important to understand the role of active species in the photocatalytic mechanism of IC degradation. The roles of $HO^{\cdot}$, $O_2^{\cdot}$-, and h^+ reactive species are significant in degradation of dye molecules [65]. The participation of reactive species were investigated by employing scavengers viz; isopropyl alcohol (IPA), benzoquinone (BQ) and EDTA to trap $HO^{\cdot}$, $O_2^{\cdot}$-, and h^+ reactive species [66] by keeping pH 10 of 10 mg L^{-1} of IC solution and catalyst dose of 1.0 % NiZrCNT at 3 mg L^{-1} (Fig. 12). Introduction of IPA had very less effect on degradation of IC proved less participation of $HO^{\cdot}$ radicals in degradation, 1 mM of BQN significantly decreased the degradation efficiency by trapping $O_2^{\cdot}$- radicals confirming the major role of this active species. The effective quenching agent of both h^+ and photo-generated electrons that is EDTA almost stopped the degradation process (even the color fading wasn't visible) further confirm the participation of $O_2^{\cdot}$- in the degradation of IC in solar light [67]. The adsorption was also decreased probably due to the formation of a catalyst-EDTA chelation complex that is blocking the contact of catalyst and dye molecules [68]. The sensitization and low recombination rate of e- / h^+ pair by MWCNT's help to generate free electrons during the degradation process and eventually generate a large amount of $O_2^{\cdot}$- in the system to enhance the degradation process [67,69]. This confirms the major role of $O_2^{\cdot}$- in the mechanism of photocatalytic degradation of IC under solar radiation.

4.6. GC–MS and TOC analysis of degraded dye solution

The degraded dye samples were subjected to solvent extraction in the diethyl ether and then the GC–MS analysis was carried out to detect the extent of degradation of dye molecules. The GC–MS studies identified various metabolites that were smaller and extensively reported in the degradation of IC dye elsewhere. Since, the degradation of organic compounds by $O_2^{\cdot}$- species is predominant and which is having powerful degradation capacity [70] many small fragments of aromatic origin were detected with dicarboxylic acids which were eventually mineralized into CO_2, H_2O, and another non-hazardous micro molecule. Fig. 13 shows the GC–MS fragments obtained from the degraded dye samples which are closely related to the reported data by various workers [71–74]. In addition, colorless molecules again investigated by TOC analysis. Fig. 14 shows TOC results for the degradation of IC dye for different intervals of time. The TOC results indicate that the concentration of IC textile dye decreased significantly with increasing time and visible light irradiation. The results confirm the effectiveness of 1.0 % NiZrCNT degradation under solar light, not only the color fading is effective but mineralization of colorless organic pollutants also achieved.

5. Comparison of the catalytic ability of ZrO_2 catalysts

Most of the work related to the ZrO_2 photocatalysts signifies the difficulties to harness maximum efficiency. The bare ZrO_2 are ineffective and take a lot of time, high catalyst quantity, extreme conditions and incorporation of heavy metals to show their ability as an effective photocatalyst [11,16,49,75]. Out of many such works Table 3.depicts few modification of ZrO_2 for betterment of ZrO_2 systems with various dopant's and contaminants with different light sources.

6. Conclusions

C,N,S, and NiCNSZrO_2/MWCNT's nanocomposites were successfully fabricated by a homogeneous co-precipitation method and were characterized by TEM in which coating of nickel doped ZrO_2 NPs is visible on MWCNT's and reveled by FT-IR spectroscopy. The XRD revealed the high crystallinity, monoclinic and tetragonal crystalline phase with successful incorporation of nickel in ZrO_2 system and EDAX confirmed the presence of non-metal and metal doping. The particle size distribution study and XRD confirmed the particle size within 5–20 nm. The highest photocatalytic activity towards indigo carmine anionic dye shown by 1 % Ni,C,*N*,S doped ZrO_2/MWCNT's which attributed to low bandgap energy, low recombination of photoinduced charge carriers and synergic effect of MWCNT's by obeying first-order rate kinetics. The reusability confirms the effectiveness of synthesized material as a photocatalyst for multiple cycles.

CRediT authorship contribution statement

Sachin Girdhar Shinde: Investigation, Writing - original draft, Conceptualization, Methodology. **Maheshkumar Prakash Patil:** Supervision, Data curation, Writing - original draft. **Gun-Do Kim:** Visualization, Investigation, Validation, Writing - review & editing. **Vinod Shankar Shrivastava:** Supervision, Validation, Writing - review & editing, Methodology, Supervision.

Declaration of Competing Interest

The authors declare that they have no known competing financial interests or personal relationships that could have appeared to influence the work reported in this paper.

Acknowledgments

The research leading to these results has received support from IIT Bombay for FT-IR, SEM, EDAX, TEM characterization, K B C North Maharashtra University, Jalgaon for XRD Characterization, SPPU University for GC–MS, MERI, Nashik for TOC analysis and Research Institute for Basic Sciences, Pukyong National University, Republic of Korea for lab facilities. Authors are also thankful to the Principal, G.T.P. College, Nandurbar and K. V. N. Naik A, C and S College, Nashik for providing necessary laboratory facilities.

References

[1] S. Natarajan, H.C. Bajaj, R.J. Tayade, Recent advances based on the synergetic effect of adsorption for removal of dyes from wastewater using photocatalytic process, J. Environ. Sci. 65 (2018) 201–222, https://doi.org/10.1016/j.jes.2017.03.011.

[2] S.S. Swati, A.N. Faruqui, Investigation on ecological parameters and COD minimization of textile effluent generated after dyeing with mono and bi-functional reactive dyes, Environ. Technol. Inno. 11 (2018) 165–173, https://doi.org/10.1016/j.eti.2018.06.003.

[3] K.B. Tan, M. Vakili, B.A. Horri, P.E. Poh, A.Z. Abdullah, B. Salamatinia, Adsorption of dyes by nanomaterials: recent developments and adsorption mechanisms, Sep. Purif. Technol. 150 (2015) 229–242, https://doi.org/10.1016/j.seppur.2015.07.

009.
[4] M. Shaban, A.M. Ashraf, Mostafa R. Abukhadra, TiO_2 Nanoribbons/Carbon nanotubes composite with enhanced photocatalytic activity; fabrication, characterization and application, Sci. Rep. 8 (2018) 781, https://doi.org/10.1038/s41598-018-19172-w.
[5] K.G. Pavithra, P.S. Kumar, V. Jaikumar, P.S. Rajan, Removal of colorants from wastewater: a review on sources and treatment strategies, J. Ind. Eng. Chem. 75 (2019) 1–19, https://doi.org/10.1016/j.jiec.2019.02.011.
[6] A. Payan, M. Fattahi, B. Roozbehani, Synthesis, characterization and evaluations of TiO_2 nanostructures prepared from different titania precursors for photocatalytic degradation of 4-chlorophenol in aqueous solution, J. Environ. Health Sci. Eng. 16 (1) (2018) 41–54, https://doi.org/10.1007/s40201-018-0295-5.
[7] L. Chen, L. Wang, X. Wu, X. Ding, A process-level water conservation and pollution control performance evaluation tool of cleaner production technology in textile industry, J. Cleaner Prod. 143 (2017) 1137–1143, https://doi.org/10.1016/j.jclepro.2016.12.006.
[8] D.B. Miklos, C. Remy, M. Jekel, K.G. Linden, J.E. Drewes, U. Hübner, Evaluation of advanced oxidation processes for water and wastewater treatment – a critical review, Water Res. 139 (2018) 118–131, https://doi.org/10.1016/j.watres.2018.03.042.
[9] P.V. Nidheesh, M. Zhou, M.A. Oturan, An overview on the removal of synthetic dyes from water by electrochemical advanced oxidation processes, Chemosphere 197 (2018) 210–227, https://doi.org/10.1016/j.chemosphere.2017.12.195.
[10] M. Bartolomeu, M.G.P.M.S. Neves, M.A.F. Faustino, A. Almeida, Wastewater chemical contaminants: remediation by advanced oxidation processes, Photochem. Photobiol. Sci. 17 (2018) 1573–1598 https://10.1039/C8PP00249E.
[11] E.S. Agorku, A.T. Kuvarega, B.B. Mamba, A.C. Pandey, A.K. Mishra, Enhanced visible-light photocatalytic activity of multi-elements-doped ZrO_2 for degradation of indigo carmine, J. of Rare Earths 33 (5) (2015) 498–506, https://doi.org/10.1016/S1002-0721(14)60447-6.
[12] S.-M. Chang, R.-A. Doong, The effect of chemical states of dopants on the microstructures and band gaps of metal-doped ZrO_2 thin films at different temperatures, J. Phys. Chem. B 108 (2004) 18098–18103, https://doi.org/10.1021/jp047440n.
[13] S.G. Botta, J.A. Navio, M.C. Hidalgo, G.M. Restrepo, M.I. Litter, Photocatalytic properties of ZrO_2 and Fe/ZrO_2 semiconductors prepared by a sol–gel technique, J. Photochem. Photobiol. A: Chem. 129 (1999) 89–99, https://doi.org/10.1016/S1010-6030(99)00150-1.
[14] C. Gionco, M.C. Paganini, M. Chiesa, S. Maurelli, S. Livraghi, E. Giamello, Cerium doped Zirconium dioxide as a potential new photocatalytic material. The role of the preparation method on the properties of thematerial, Appl. Catal. A 504 (2015) 338–343, https://doi.org/10.1016/j.apcata.2015.02.021.
[15] W.-S. Dong, K.-W. Jun, H.-S. Roh, Z.-W. Liu, S.-E. Park, Comparative study on partial oxidation of methane over Ni/ZrO_2, Ni/CeO_2 and Ni/Ce–ZrO_2 catalysts, Catal. Lett. 78 (1–4) (2002) 215–222, https://doi.org/10.1016/j.apcata.2015.02.021.
[16] A. Shojaie, M. Fattahi, S. Jorfi, B. Ghasemi, Synthesis and evaluations of Fe_3O_4–TiO_2–Ag nanocomposites for photocatalytic degradation of 4-chlorophenol (4-CP): effect of Ag and Fe compositions, Int. J. Ind. Chem. Biotechnol. 9 (2018) 141–151, https://doi.org/10.1007/s40090-018-0145-4.
[17] A. Shojaie, M. Fattahi, S. Jorfi, B. Ghasemi, Hydrothermal synthesis of Fe-TiO_2-Ag nano-sphere for photocatalytic degradation of 4-chlorophenol (4-CP): investigating the effect of hydrothermal temperature and time as well as calcination temperature, J. Environ. Chem. Eng. 5 (5) (2017) 564–4572, https://doi.org/10.1016/j.jece.2017.07.024.
[18] A. Shojaie, M. Fattahi, S. Jorfi, B. Ghasemi, Synthesis and evaluations of Fe_3O_4–TiO_2–Ag nanocomposites for photocatalytic degradation of 4-chlorophenol (4-CP): effect of Ag and Fe compositions, Int. J. Ind. Chem. Biotechnol. 9 (2) (2018) 141–151, https://doi.org/10.1007/s40090-018-0145-4.
[19] X. Zou, X. Dong, L. Wang, H. Ma, X. Zhang, X. Zhang, Preparation of Ni doped ZnO-TiO_2 composites and their enhanced photocatalytic activity, Int. J. Photoenergy (2014), https://doi.org/10.1155/2014/893158.
[20] X. Yue, S. Yi, R. Wang, Z. Zhang, S. Qiu, Cadmium sulfide and nickel synergetic Co-catalysts supported on graphitic carbon nitride for visible-light-Driven photocatalytic hydrogen evolution, Sci. Rep. 6 (2016) 22268, https://doi.org/10.1038/srep22268.
[21] G. Poungchan, B. Ksapabutr, M. Panapoy, One-step synthesis of flower-like carbon-doped ZrO_2 for visible-light-responsive photocatalyst, Mater. Des. 89 (2016) 137–145, https://doi.org/10.1016/j.matdes.2015.09.136.
[22] K.Qi.B. Cheng, J. Yu, W. Ho, Review on the improvement of the photocatalytic and antibacterial activities of ZnO, J. Alloys. Compd. 727 (2017) 792–820, https://doi.org/10.1016/j.jallcom.2017.08.142.
[23] R. Ashouri, P. Ghasemipoor, B. Rasekh, F. Yazdian, S.R. Mofradnia, M. fattahi, The effect of ZnO-based carbonaceous materials for degradation of benzoic pollutants: a review, Int. J. Environ. Sci. Technol. (Tehran) 3 (16) (2019) 1729–1740, https://doi.org/10.1007/s13762-018-2056-5.
[24] M. Fattahi, M. Kazemeini, F. Khorasheh, A.M. Rashidi, Vanadium pentoxide catalyst over carbon-based nanomaterials for the oxidative dehydrogenation of propane, Ind. Eng. Chem. Res. 52 (46) (2013) 16128–16141, https://doi.org/10.1021/ie4007358.
[25] M. Fattahi, M. Kazemeini, F. Khorasheh, A.M. Rashidi, Morphological Investigations of Nanostructured V_2O5 over Graphene Used for the ODHP Reaction: From Synthesis to Physiochemical Evaluations, Catal. Sci. Technol. 5 (2015) 910–924, https://doi.org/10.1039/C4CY01108B.
[26] F. Hayati, A.A. Isari, M. Fattahi, B. Anvaripour, S. Jorfi, Photocatalytic decontamination of phenol and petrochemical wastewater through ZnO/TiO_2 decorated on reduced graphene oxide nanocomposite: influential operating factors,mechanism, and electrical energy consumption, RSC Adv. 8 (2018) 40035–40053, https://doi.org/10.1039/c8ra07936f.
[27] A.A. Isari, A. Payan, M. Fattahi, S. Jorfi, B. Kakavandi, Photocatalytic degradation of Rhodamine B and Real Textile Wastewater using Fe-Doped TiO_2 anchored on reduced Graphene Oxide (Fe-TiO_2/rGO):characterization and feasibility, mechanism and pathway studies, Appl. Surf. Sci. 462 (2018) 549–564, https://doi.org/10.1016/j.apsusc.2018.08.133.
[28] R. Shahbazi, A. Payan, M. Fattahi, Preparation, evaluations and operating conditions optimization of nano TiO_2 over graphene based materials as the photocatalyst for degradation of phenol, J. Photochem. Photobiol. A: Chem. 364 (2018) 564–576, https://doi.org/10.1016/j.jphotochem.2018.05.032.
[29] F. Hayati, A.A. Isari, B. Anvaripour, M. Fattahi, B. Kakavandi, Ultrasound-assisted photocatalytic degradation of sulfadiazine using MgO@CNT heterojunction composite: effective factors, pathway and biodegradability studies, Chem. Eng. J. 381 (2020) 122636, , https://doi.org/10.1016/j.cej.2019.122636.
[30] D. Chaudhary, N. Khare, V.D. Vankar, Ag nanoparticles loaded TiO_2/MWCNT ternary nanocomposite: a visible-light-driven photocatalyst with enhanced photocatalytic performance andstability, Ceram. Int. 42 (14) (2016) 15861–15867, https://doi.org/10.1016/j.ceramint.2016.07.056.
[31] Y.-H. Tseng, C.-Y. Yen, M.-Y. Yen, C.-C.M. Ma, Effects of the acid pretreated multi-walled carbon nanotubes on the photocatalytic capacity of TiO_2/multi-walled carbon nanotubes nanocomposites, Micro Nano Lett. 5 (1) (2010) 1–6, https://doi.org/10.1049/mnl.2009.0094.
[32] A. Anson, J. Jagiello, J.B. Parra, M.L. Sanjuan, A.M. Benito, W.K. Maser, M.T. Martinez, Porosity, surface area, surface energy, and hydrogen adsorption in nanostructured carbons, J. Phys. Chem. B 108 (2004) 15820–15826, https://doi.org/10.1021/jp047253p.
[33] S.G. Shinde, M.P. Patil, G.-D. Kim, V.S. Shrivastava, Multi-doped ZnO photocatalyst for solar induced degradation of Indigo Carmine Dye and as an antimicrobial agent, J. Inorg. Organomet. Polym. Mater. (2019) 1–12, https://doi.org/10.1007/s10904-019-01273-2.
[34] F. Pei, Y. Liu, S. Xu, J. Lu¨, C. Wang, S. Cao, Nanocomposite of graphene oxide with nitrogen doped TiO_2 exhibiting enhanced photocatalytic efficiency for hydrogen evolution, Int. J. Hydrogen Energy 38 (6) (2013) 2670–2677, https://doi.org/10.1016/j.ijhydene.2012.12.045.
[35] Q. Mahmood, A. Afzal, H.M. Siddiqi, A. Habib, Sol–gel synthesis of tetragonal ZrO_2 nanoparticles stabilized by crystallite size and oxygen vacancies, J. Solgel Sci. Technol. 67 (3) (2013) 670–674, https://doi.org/10.1007/s10971-013-3112-8.
[36] S. Jayakumar, P.V. Ananthapadmanabhan, K. Perumal, T.K. Thiyagarajan, S.C. Mishra, L.T. Su, A.I.Y. Tok, J. Guo, Characterization of nano-crystalline ZrO_2 synthesized via reactive plasma processing, Mater. Sci. Eng., B 176 (2011) 894–899, https://doi.org/10.1016/j.mseb.2011.05.013.
[37] C. Gionco, M.C. Paganini, E. Giamello, O. Sacco, V. Vaiano, Diana Sannino, Rare earth oxides in zirconium dioxide: how to turn a wide band gap metal oxide into a visible light active photocatalyst, J. Energy Chem. 26 (2) (2017) 270–276, https://doi.org/10.1016/j.jechem.2016.07.006.
[38] H. Yan, D. Zhang, J. Xu, Y. Lu, Y. Liu, K. Qiu, Y. Zhang, Y. Luo, Solution growth of NiO nanosheets supported on Ni foam as high-performance electrodes for Supercapacitors, Nanoscale Res. Lett. 9 (424) (2014) 1–7, https://doi.org/10.1186/1556-276X-9-424.
[39] S.N. Basahel, T.T. Ali, M. Mokhtar, K. Narasimharao, Influence of crystal structure of nanosized ZrO_2 on photocatalytic degradation of methyl orange, Nanoscale Res. Lett. 10 (73) (2015) 1–13, https://doi.org/10.1186/s11671-015-0780-z.
[40] F.A. Harraz, R.M. Mohamed, A. Shawky, I.A. Ibrahim, Composition and phase control of Ni/NiO nanoparticles for photocatalytic degradation of EDTA, J. Alloys. Compd. 508 (2010) 133–140, https://doi.org/10.1016/j.jallcom.2010.08.027.
[41] S. Tagmouti, S.E. Bouzit, L.C. Costa, M.P.F. Graça, A. Outzourhit, Impedance spectroscopy of nanofluids based on multiwall carbon nanotubes, Spectrosc. Lett. 48 (10) (2015) 761–766, https://doi.org/10.1080/00387010.2015.1034874.
[42] Y. Chang, C. Wang, T. Liang, C. Zhao, X. Luo, T. Guo, J. Gong, H. Wu, Sol–gel synthesis of mesoporous spherical zirconia, RSC Adv. 5 (2015) 104629–104634, https://doi.org/10.1039/C5RA23782C.
[43] S. Onsuratoom, T. Puangpetch, S. Chavadej, Comparative investigation of hydrogen production over Ag, Ni and Cu-loaded mesoporous-assembled TiO_2–ZrO_2 mixed oxide nanocrystal photocatalysts, Chem. Eng. J. 173 (2011) 667–675, https://doi.org/10.1016/j.cej.2011.08.016.
[44] Z. Wang, J. Xia, Y. Xia, C. Lu, G. Shi, F. Zhang, F. Zhu, Y. Li, L. Xia, J. Tang, Fabrication and characterization of a zirconia/multi-walled carbon nanotube mesoporous composite, Mater. Sci. Eng. C. 33 (2013) 3931–3934, https://doi.org/10.1016/j.msec.2013.05.031.
[45] C.G. Silva, J.L. Faria, Photocatalytic oxidation of benzene derivatives in aqueous suspensions:synergic effect induced by the introduction of carbon nanotubes in a TiO_2 matrix, Appl. Catal. B 101 (2010) 81–89, https://doi.org/10.1016/j.apcatb.2010.09.010.
[46] T. Sreethawong, S. Ngamsinlapasathian, S. Yoshikawa, Synthesis of crystalline mesoporous-assembled ZrO_2 nanoparticles via a facile surfactant-aided sol–gel process and their photocatalytic dye degradation activity, Chem. Eng. J. 228 (2013) 256–262, https://doi.org/10.1016/j.cej.2013.04.111.
[47] Hanggara Sudrajat, Sandhya Babel, Hiroshi Sakai, Satoshi Takizawa, Rapid enhanced photocatalytic degradation of dyes using novel N-doped ZrO_2, J. Environ. Manage. 165 (2016) 224–234, https://doi.org/10.1016/j.jenvman.2015.09.036.
[48] H.C. Madhusudhana, S.N. Shobhadevi, B.M. Nagabhushana, B.V. Chaluvaraju, M.V. Murugendrappa, R. Hari Krishna, H. Nagabhushana, N.R. Radeep, Effect of fuels on conductivity, dielectric and humidity sensing properties of ZrO_2 nanocrystals prepared by low temperature solution combustion method, J. Asian Ceram. Soc. 4 (3) (2016) 309–318, https://doi.org/10.1016/j.jascer.2016.05.009.

[49] B.R. Singh, M. Shoeb, W. Khan, A.H. Naqvi, Synthesis of graphene/zirconium oxide nanocomposite photocatalyst for the removal of rhodamine B dye from aqueous environment, J. Alloys. Compd. 651 (2015) 598–607, https://doi.org/10.1016/j.jallcom.2015.05.231.

[50] B.P. Singh, V. Choudhary, S. Teotia, T.K. Gupta, V.N. Singh, S.R. Dhakate, R.B. Mathur, Solvent free, efficient, industrially viable, fast dispersion process based amine modified MWCNT reinforced epoxy composites of superior mechanical properties, Adv. Mater. Lett. 6 (2) (2015) 104–113, https://doi.org/10.5185/amlett.2015.5612.

[51] J.M.E. Matos, F.M.A. Júnior, L.S. Cavalcante, V. Santos, S.H. Leal, L.S.S. Júnior, M.R.M.C. Santos, E. Longo, Reflux synthesis and hydrothermal processing of ZrO_2 nanopowders at low temperature, Mater. Chem. Phys. 117 (2009) 455–459, https://doi.org/10.1016/j.matchemphys.2009.06.024.

[52] B. Molki, W.M. Aframehr, R. Bagheri, J. Salimi, Mixed matrix membranes of polyurethane with nickel oxide nanoparticles for CO_2 gas separation, J. Membr. Sci. 549 (2018) 588–601, https://doi.org/10.1016/j.memsci.2017.12.056.

[53] G.K. Sidhu, A.K. Kaushik, S. Rana, S. Bhansali, R. Kumar, Photoluminescence quenching of Zirconia nanoparticle by surface modification, Appl. Surf. Sci. 334 (2015) 216–221, https://doi.org/10.1016/j.apsusc.2014.10.036.

[54] D. Wu, Z. Zhang, W. Fu, X. Fan, H. Guo, Structure, electrical and chemical properties of zirconium nitride films deposited by dc reactive magnetron sputtering, Appl. Phys. A 64 (1997) 593–595, https://doi.org/10.1007/s003390050522.

[55] Z. Barhon, F. Bozon-Verduraz, N. Saffaj, A. Albizane, Mohamed Azzi, Mohamed Kacimi, M. Ziyad, Photodegradation of Indigo carmine in aqueous solution by zirconium phosphates, Desalin. Water Treat. 30 (1-3) (2011) 69–73, https://doi.org/10.5004/dwt.2011.1394.

[56] K. Byrappa, A.S. Dayananda, C.P. Sajan, B. Basavalingu, M.B. Shayan, K. Soga, M. Yoshimura, Hydrothermal preparation of ZnO:CNT and TiO_2:CNT composites and their photocatalytic applications, J. Mater. Sci. 43 (2008) 2348–2355, https://doi.org/10.1007/s10853-007-1989-8.

[57] S.D. Khairnar, V.S. Shrivastava, Photocatalytic degradation of chlorpyrifos and methylene blue using α-Bi_2O_3 nanoparticles fabricated by sol–gel method, SN Appl. Sci. 1 (2019) 762, https://doi.org/10.1007/s42452-019-0761-4.

[58] M.S. Abdel-wahab, A. Jilani, I.S. Yahia, A.A. Al-Ghamdi, Enhanced the photocatalytic activity of Ni-doped ZnO thin films: morphological, optical and XPS analysis, Superlattices Microstruct. 94 (2016) 108–118, https://doi.org/10.1016/j.spmi.2016.03.043.

[59] A. Di Mauro, M.E. Fragalà, V. Privitera, G. Impellizzeri, ZnO for application in photocatalysis: from thin films to nanostructures, Mater. Sci. Semicond. Process. 69 (2017) 44–51, https://doi.org/10.1016/j.mssp.2017.03.029.

[60] M.H. Farzana, S. Meenakshi, Synergistic effect of chitosan and titanium dioxide on the removal of toxic dyes by the photodegradation technique, Ind. Eng. Chem. Res. 53 (2014) 55–63, https://doi.org/10.1021/ie402347g.

[61] S.-M. Chang, R.-an Doong, The effect of chemical states of dopants on the microstructures and band gaps of metal-doped ZrO_2 thin films at different temperatures, J. Phys. Chem. B 108 (2004) 18098–18103, https://doi.org/10.1021/jp047440n.

[62] C.M. Magdalane, K. Kaviyarasu, J.J. Vijaya, C. Jayakumar, M. Maaza, B. Jeyaraj, Photocatalytic degradation effect of malachite green and catalytic hydrogenation by UV–illuminated CeO_2/CdO multilayered nanoplatelet arrays: investigation of antifungal and antimicrobial activities, J. Photochem. Photobiol. B 169 (2017) 110–123, https://doi.org/10.1016/j.jphotobiol.2017.03.008.

[63] M. Bahrami, A. Nezamzadeh-Ejhieh, Effect of supporting and hybridizing of FeO and ZnO semiconductors onto an Iranian clinoptilolite nano-particles and the effect of ZnO/FeO ratio in the solar photodegradation of fish ponds waste water, Mater. Sci. Semicond. Process. 27 (2014) 833–840, https://doi.org/10.1016/j.mssp.2014.08.030.

[64] Y. Ni, S. Chena, S. Kokot, Spectrophotometric determination of metal ions in electroplating solutions in the presence of EDTA with the aid of multivariate calibration and artificial neural networks, Anal. Chim. Acta 463 (2002) 305–316, https://doi.org/10.1016/S0003-2670(02)00437-3.

[65] M. Pera-Titus, V. Garcia-Molina, Miguel A. Baños, J. Giménez, S. Esplugas, Degradation of chlorophenols by means of advanced oxidation processes: a general review, Appl. Catal. B 47 (2004) 219–256, https://doi.org/10.1016/j.apcatb.2003.09.010.

[66] K. Rajeshwar, M.E. Osugi, W. Chanmanee, C.R. Chenthamarakshan, M.V.B. Zanoni, P. Kajitvichyanukul, R. Krishnan-Ayer, Heterogeneous photocatalytic treatment of organic dyes in air and aqueous media, J. Photochem. Photobiol. C Photochem. Rev. 9 (2008) 171–192, https://doi.org/10.1016/j.jphotochemrev.2008.09.001.

[67] G. Mamba, M.A. Mamo, X. Mbianda, A.K. Mishra, Nd,N,S-TiO_2 decorated on reduced graphene oxide for a highly efficient visible light active photocatalyst for dye degradation: a comparison to its MWCNT/Nd,N,S-TiO_2 analogue, Ind. Eng. Chem. Res. 53 (37) (2014) 14329–14338, https://doi.org/10.1021/ie502610y.

[68] S. Akshatha, S. Sreenivasa, L. Parashuram, V. Udaya, Kumar, S.C. Sharma, H. Nagabhushana, Sandeep Kumar, T. Maiyalagan, Synergistic effect of hybrid Ce^{3+}/Ce^{4+} doped Bi_2O_3 nano-sphere photocatalyst for enhanced photocatalytic degradation of alizarin red S dye and its NUV excited photoluminescence studies, J. Environ. Chem. Eng. 7 (3) (2019) 103053, , https://doi.org/10.1016/j.jece.2019.103053.

[69] X. Wu, Y. Si, J. Yu, B. Ding, Titania-based electrospun nanofibrous materials: a new model for organic pollutants degradation, MRS Commun. 8 (3) (2018) 765–781, https://doi.org/10.1557/mrc.2018.139.

[70] M. Vautier, C. Guillard, J.-M. Herrmann, Photocatalytic degradation of dyes in water: case study of indigo and of indigo carmine, J. Catal. 201 (2001) 46–59, https://doi.org/10.1006/jcat.2001.3232.

[71] J. Terres, R. Battisti, J. Andreaus, P. Cesar De Jesus, Decolorization and degradation of Indigo Carmine dye from aqueous solution catalyzed by horseradish peroxidase, Biocatal. Biotransform. 32 (1) (2014) 64–73, https://doi.org/10.3109/10242422.2013.873416.

[72] F.V. de Andrade, G.M. de Lima, R. Augusti, M.G. Coelho, J.D. Ardisson, O.B. Romero, A versatile approach to treat aqueous residues of textile industry: the photocatalytic degradation of Indigo Carmine dye employing the autoclaved cellular concrete/Fe_2O_3 system, Chem. Eng. J. 180 (2012) 25–31, https://doi.org/10.1016/j.cej.2011.10.089.

[73] M.L. Chacón-Patiño, C. Blanco-Tirado, J.P. Hinestroza, Marianny Y. Combariza, Biocomposite of nanostructured MnO_2 and fique fibers for efficient dye degradation, Green Chem. 15 (2013) 2920–2928, https://doi.org/10.1039/C3GC40911B.

[74] S.R. Teeparthi, E.W. Awin, R. Kumar, Dominating role of crystal structure over defect chemistry in black and white zirconia on visible light photocatalytic activity, Sci. Rep. 8 (1) (2018) 1–11, https://doi.org/10.1038/s41598-018-23648-0.

[75] T.E. Agustina, H.M. Ang, V.K. Vareek, A review of synergistic effect of photocatalysis and ozonation on wastewater treatment, J. Photochem. Photobiol. C Photochem. Rev. 6 (2005) 264–273, https://doi.org/10.1016/j.jphotochemrev.2005.12.003.

[76] A. Nodehi, H. Atashi, M. Mansouri, Improved photocatalytic degradation of reactive blue 81 using NiO-doped ZnO–ZrO_2 nanoparticles, J. Dispersion Sci. Technol. 40 (5) (2019) 766–776, https://doi.org/10.1080/01932691.2018.1499522.

[77] M. Mzoughi, W.W. Anku1, S.O.B. Oppong, S.K. Shukla, E.S. Agorku, P.P. Govender, Neodymium doped ZrO_2-graphene oxide nanocomposites: a promising photocatalyst for photodegradation of Eosin Y dye, Adv. Mater. Lett. 7 (12) (2016) 946–950, https://doi.org/10.5185/amlett.2016.6497.

[78] M. Rahimi-Nasrabadi, H. Ehrlich, F. Sedighi, Tailored synthesis of Sm_2O_3 and Eu_2O_3 doped ZrO_2 nanoparticles: photodegaradtion of p-nitrpophenol in water, J. Mater. Sci. : Mater. Electron. 29 (2018) 11081, https://doi.org/10.1007/s10854-018-9190-1.

[79] K. Saeed, M. Sadiq, I. Khan, S. Ullah, N. Ali, A. Khan, Synthesis, characterization, and photocatalytic application of Pd/ZrO_2 and Pt/ZrO_2, Appl. Water Sci. 8 (2018) 60, https://doi.org/10.1007/s13201-018-0709-7.

[80] G. Ravi, S. Palla, J.R. Reddy, N.K. Veldurthi, B.V. Kumar, M. Vithal, Photocatalytic and conductivity studies of Bi^{3+} substituted $La_2Zr_2O_7$, Int. J. Green Nanotechnol. 4 (2012) 360–367, https://doi.org/10.1080/19430892.2012.738145.

[81] A.I. Vaizogullar, A. Balci, M. Ugurlu, Synthesis of ZrO_2 and ZrO_2/SiO_2 particles and photocatalytic degradation of methylene blue, Indian J. Chem. 54 A (2015) 1434–1439 http://hdl.handle.net/123456789/33506.